Radiative Effects of Cloud Inhomogeneity and Geometric Association Over the Tropical Western Pacific Warm Pool

X. Wu
National Center for Atmospheric Research[(a)]
Boulder, Colorado

X. -Z. Liang
Illinois State Water Survey
Champaign, Illinois

Introduction

The representation of cloud systems and cloud-radiation interaction is considered to be one of major uncertainties in general circulation models (GCMs). This arises because (1) complete observations of cloud systems are impossible and available measurements are very limited; (2) cloud-radiation interactions are scale-dependent (Dudek et al. 1996) while current GCMs cannot explicitly resolve them (Wu and Moncrieff 2001a); and (3) conventional GCM parameterizations of cloud-radiation interactions are inadequate and model results strongly depend on cloud-overlap assumptions and optical property approximations (Del Genio et al. 1996; Fowler and Randall 1996; Liang and Wang 1997).

While GCMs require convection and cloud parameterizations, cloud-resolving models (CRMs) explicitly resolve convection and mesoscale organization, where cloud microphysical processes and cloud-radiation interactions directly respond to the cloud-scale dynamics. Wu and Moncrieff (2001a) demonstrated that the CRM produces vertical and horizontal distributions of cloud liquid and ice that interact much more realistically with radiation than the single-column model (SCM) of the National Center for Atmospheric Research (NCAR) Community Climate Model, Version 3 (CCM3), where the radiative effect is calculated from a single volume of "effective" cloud. In most GCM parameterizations of cloud-radiation interactions, clouds are assumed to be horizontally homogeneous and the vertical cloud geometric association is treated by the cloud-overlap assumptions (Liang and Wang 1997). Consequently, the CRM simulation can get the top of the atmosphere (TOA) and surface net shortwave (SW) fluxes to agree simultaneously with observations from the Tropical Ocean Global Atmosphere (TOGA) Coupled Ocean Atmosphere Response Experiment (COARE), whereas GCMs and SCMs generally fail to do so. To reduce the uncertainties, we will attempt to utilize CRM integrations, validated by the Atmospheric Radiation Measurement (ARM) Program (e.g., Mace et al. 1998; Ackerman et al. 1999), to develop cloud statistics and improve the treatment of subgrid cloud-radiation interactions in GCMs.

(a) The NCAR is sponsored by the National Science Foundation.

Radiative Effects of Subgrid Cloud Variability

Given the successful verification of CRM integrations against various observations (e.g., Wu et al. 1998, 1999), the CRM and SCM integrations are compared to identify and isolate the cause of uncertainties such as the bias in the net surface energy budget in GCMs (Wu and Moncrieff 2001a). Convection and clouds are directly resolved in the CRM, while they are represented separately (not necessarily in a consistent way) by parameterizations in the SCM (e.g., Wu and Moncrieff 2001b). It is demonstrated that the CRM surface energy budgets and TOA radiative fluxes simultaneously agree with the TOGA-COARE observations within the measurement uncertainty, while the corresponding quantities derived from the SCM have large biases.

Table 1 compares the simulated and observed surface energy budgets averaged over the 30-day period. The net surface longwave (LW), SW, latent heat, and sensible heat fluxes from the CRM are in excellent agreement with the observations, each difference being smaller than 5 Wm^{-2}. The difference between the CRM and observed net surface fluxes is 2.6 Wm^{-2}. On the other hand, there is a large discrepancy between the SCM and observations, especially in the net SW radiative flux and latent heat flux.

Table 1. Surface energy budgets from observations (OBS and SSM/I/GMS), the CRM and SCM, averaged over the 30-day period from December 5, 1992, to January 3, 1993. The OBS are averaged from three ships and a buoy.

Fluxes (W m^{-2})	OBS	SSM/I/GMS	CRM M0	SCM	ECMWF
Q_{LW}(SRF)	-51.6	-48.2	-48.2	-57.0	-57.3
Q_{SW}(SRF)	178.6	173.2	179.3	227.7	206.2
Q_{lat}	-122.9	-126.9	-125.2	-139.3	-145.1
Q_{sen}	-10.3	-7.7	-9.5	-11.1	-11.7
Q_{net}	-6.2	-9.6	-3.6	20.3	-7.9

$$Q_{net} = Q_{LW}(SRF) + Q_{SW}(SRF) + Q_{lat} + Q_{sen}$$

Q_{LW}(SRF) = net LW flux
Q_{SW}(SRF) = net SW flux
Q_{lat} = latent heat flux
Q_{sen} = sensible heat flux
OBS = observed fluxes
SSM/I = special sensor microwave/imager
GMS = geostationary meteorological satellite

Table 2 shows the 30-day averaged TOA radiative fluxes from the CRM, SCM, and three observational estimates. In terms of the net LW flux, the CRM flux is about 5 Wm^{-2} less than the observations, while the SCM is about 10 Wm^{-2} larger than the observed fluxes. The European Centre for Medium-Range Weather Forecasts (ECMWF) flux is even larger, which suggests an underprediction of cloud amounts during the 30-day period. For the net SW flux, the CRM is in good agreement with the FC and GMS2, but smaller than the GMS1. The SW fluxes from the SCM and ECMWF are larger than all three estimates, but closer to the GMS1.

Table 2. TOA radiative fluxes from observations (FC, GMS1, and GMS2), the CRM and SCM, averaged over the period of 30 days. The Flux and Cloud (FC) data is derived from a radiative transfer model using the satellite-measured radiance and the cloud properties obtained from International Satellite Cloud Climatology Program (ISCCP). The GMS1 is produced by the calibration of surface instruments against collocated observations from the NASA ER-2 Aircraft. The GMS2 is estimated by using an empirically obtained narrowband-broadband relationship from simultaneous satellite measurements.

Fluxes (W m^{-2})	FC	GMS1	GMS2	CRM M0	SCM	ECMWF
Q_{LW}(TOA)	-198.8	-200.4	-205.1	-195.8	-211.7	-246.9
Q_{SW}(TOA)	269.5	294.4	274.4	274.8	312.4	307.7

Using the CRM simulation as a benchmark, two offline radiation calculations are conducted to quantify the effects of the overlap assumption and the subgrid cloud horizontal variability on the radiative fluxes using the CRM-produced month-long cloud-scale temperature, moisture, and condensate fields.

In the full CRM (M0), the so-called binary clouds (i.e., completely overcast or clear skies) are used for 300 columns. We define a grid box at a given level to be completely overcast if the sum of liquid and ice water path exceeds threshold 0.2 g m^{-2}. The radiative flux is calculated for each column using the radiative transfer model, and the 300 columns are then averaged to get the mean radiative flux. The radiative effect of subgrid cloud horizontal (inhomogeneity) and vertical (geometric association) distribution is thereby explicitly included in the CRM-produced radiative flux.

The offline calculation M2 is designed to estimate the impact of cloud inhomogeneity on the radiative flux. For each completely overcast column at a given level, the cloud radiative properties (including cloud amount, emissivity, extinction optical depth, single scattering albedo, asymmetry parameter, and forward scattered fraction) are replaced by the domain-averaged value. As in M0, the radiative transfer is calculated for each column and the mean radiative flux is obtained by averaging all 300 columns. For M2, only the horizontal inhomogeneity is removed (Figure 1), while all others (including temperature and water vapor profiles) are kept identical to M0. Thus, the differences between M0 and M2 represent the effect of cloud horizontal inhomogeneity.

As shown in Table 3, the difference between M0 and M2 is more than 30 Wm^{-2} for the SW flux and more than 10 Wm^{-2} for the TOA LW flux. The removal of the cloud inhomogeneity is to reduce the domain-averaged SW and LW fluxes. This result indicates that the CCM3 radiation scheme, like many GCM parameterizations of cloud-radiation interactions that assume clouds are horizontally homogeneous, can substantially underestimate the radiative flux, especially the SW flux.

In the offline calculation M1, the mean cloud radiative properties and cloud fraction profiles are obtained from the 300 columns of the CRM domain; the radiative flux is then calculated using the mean profile. In this case, the cloud vertical distribution has to be treated by the cloud-overlap assumptions because there is only one column for each time step. So M1 is the same as what the SCM is doing except the cloud amount and cloud fraction profiles are from the CRM. Because the mean cloud radiative properties are the same for M1 and M2, the difference between M2 and M1 (Table 3) is due to the effect of the cloud-overlap assumption (a random overlap assumption currently used in the

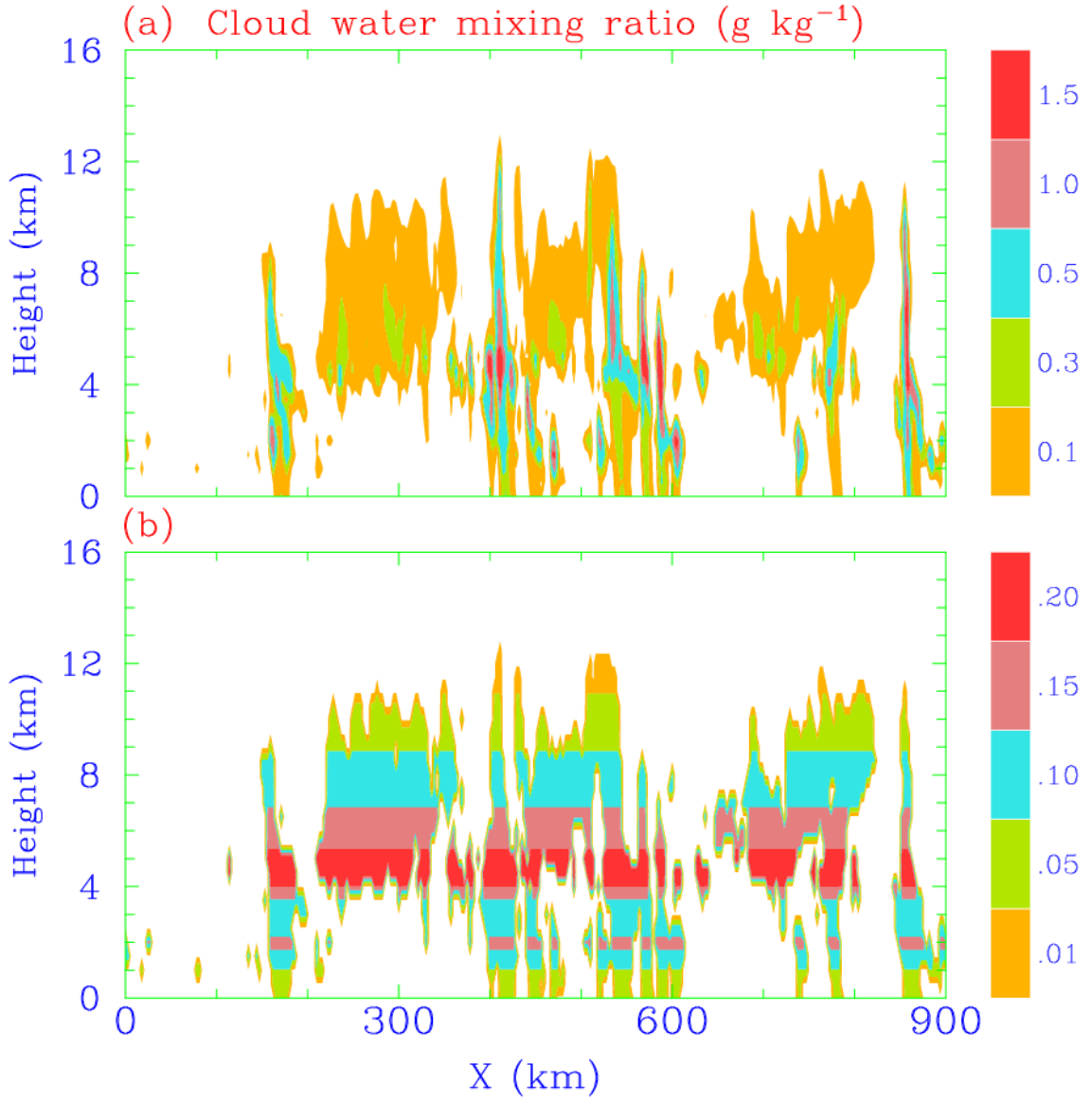

Figure 1. (a) Snapshot of the cloud: water mixing ratio (g kg^{-1}) in 1230 Universal Time Coordinates December 22, 1992, (b) same as (a) but the horizontal inhomogeneity is removed.

Table 3. 30-day mean TOA and surface (SRF) radiative fluxes from the CRM (M0) and offline radiation calculations (M1 and M2).

Fluxes (W m-2)	CRM M0	M2 (M0-M2)	M1 (M2-M1)
Q_{LW}(TOA)	-195.8	-182.6 (-13.2)	-171.2 (-11.4)
Q_{LW}(SRF)	-48.2	-46.4 (-1.8)	-39.3 (-7.1)
Q_{SW}(TOA)	274.8	243.6 (31.2)	238.4 (5.2)
Q_{SW}(SRF)	179.3	145.9 (33.4)	141.1 (4.8)

CCM3 radiation scheme). The random overlap assumption tends to overestimate the total cloud cover, which results in smaller SW and LW fluxes in M1 than in M2 (e.g., Tian and Curry 1989; Liang and Wang 1997).

Statistics of Subgrid Cloud Variability

We have constructed some preliminary cloud statistics from both the ARM measurements at Southern Great Plains (SGP) and a 30-day (December 5, 1992 - January 3, 1993) CRM integration of cloud systems during TOGA-COARE. The CRM data have 3-km horizontal grid spacing covering the 900-km domain (Wu et al. 1998). The SGP data are satellite measurements for $(50\ km)^2$ pixels within a $(100\ km)^2$ grid area during the period of April 6-30, 1994 (Dudek et al. 1996).

Figure 2 shows there is substantial subgrid variability of cloud radiative forcing within a GCM grid. The difference between the ARM and CRM may arise from different cloud regimes at the SGP and TOGA-COARE. This will be verified using the ARM measurements at the Tropical Western Pacific (TWP). Nonetheless, both data indicate a large spread of cloud radiative forcing for a given GCM-grid mean. This subgrid variability may not likely be resolved by a single volume of "effective" cloud. The mosaic treatment will provide a solution.

Figure 3 shows the cloud vertical distributions constructed from the CRM integrations during TOGA-COARE. The statistics indicate that clouds occur 54% of the time in single (penetrative) towers, 12% in two distinct cells, and 4% at multiple levels. Most of the penetrative clouds have a peak of water content at 6 km, where ice formation is maximized near the local temperature -10°C. There is a secondary peak at 4.5 km, where liquid water growth reaches the maximum above the updraft mass flux maxima. Note that the peak concentration of cloud water is independent of the cloud base height, which is different from the exponential decaying vertical profile adopted by the CCM3.

Mosaic Treatment of Subgrid Cloud-Radiation Interactions

The first version of the mosaic treatment has been developed and applied to two separate GCM platforms (Liang and Wang 1997). The critical issue identified in the development is how the vertical cloud distribution at each GCM grid is grouped into subcells to realistically treat geometric structures and their associations. Current GCMs predict major cloud genera (convective C_c, anvil cirrus C_i, and stratiform C_s) amounts as overall fractional coverage of the model grid in individual layers without explicitly specifying their spatial associations. In contrast, the mosaic treatment divides the GCM grid into multiple subcells (Figure 4) so that an individual layer within the subcell is either completely overcast or cloud free (i.e., binary cloud). Each overcast subcell layer contains a specific cloud genus with distinct optical properties. Clouds with and without geometric associations are distinguished and vertically blended through the use of maximum and random overlaps, respectively.

One interesting aspect of the mosaic approach is the "stochastic" cloud radiative forcing that results from the special treatment for C_s clouds. Adjacent layers that contain C_s are vertically aligned by an identical set of random-order subcells to acquire a maximum overlap, whereas discrete C_s layers use an independent set (i.e., generated randomly each time) to treat the overlap, thus producing the stochastic

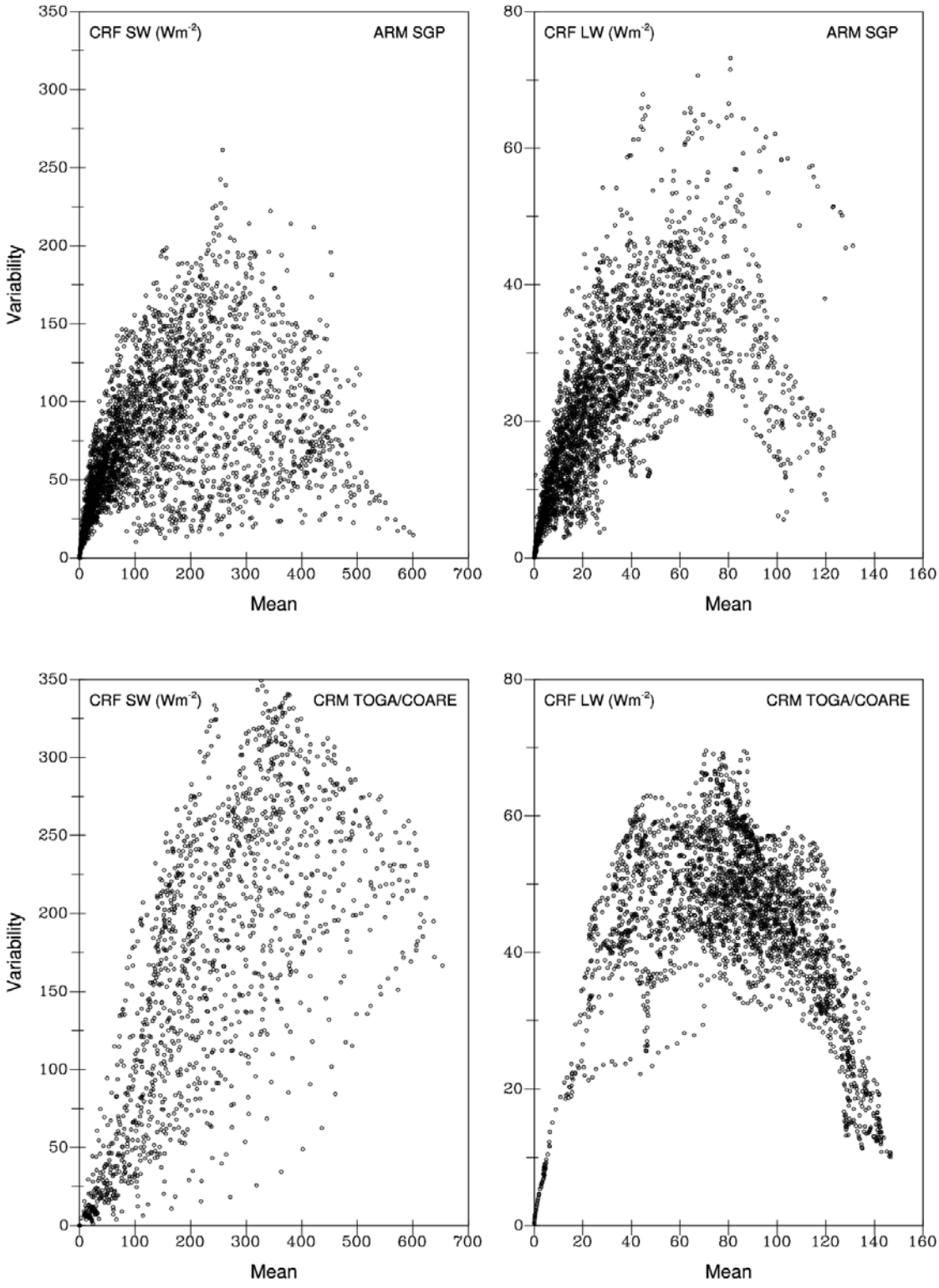

Figure 2. Scatter diagrams between grid means (abscissa) and mesoscale deviations (ordinate) of TOA cloud-radiation forcing (SW = shortwave; LW = longwave). The upper panel is for the SGP data, and the lower panel is for the CRM data (see text for the description).

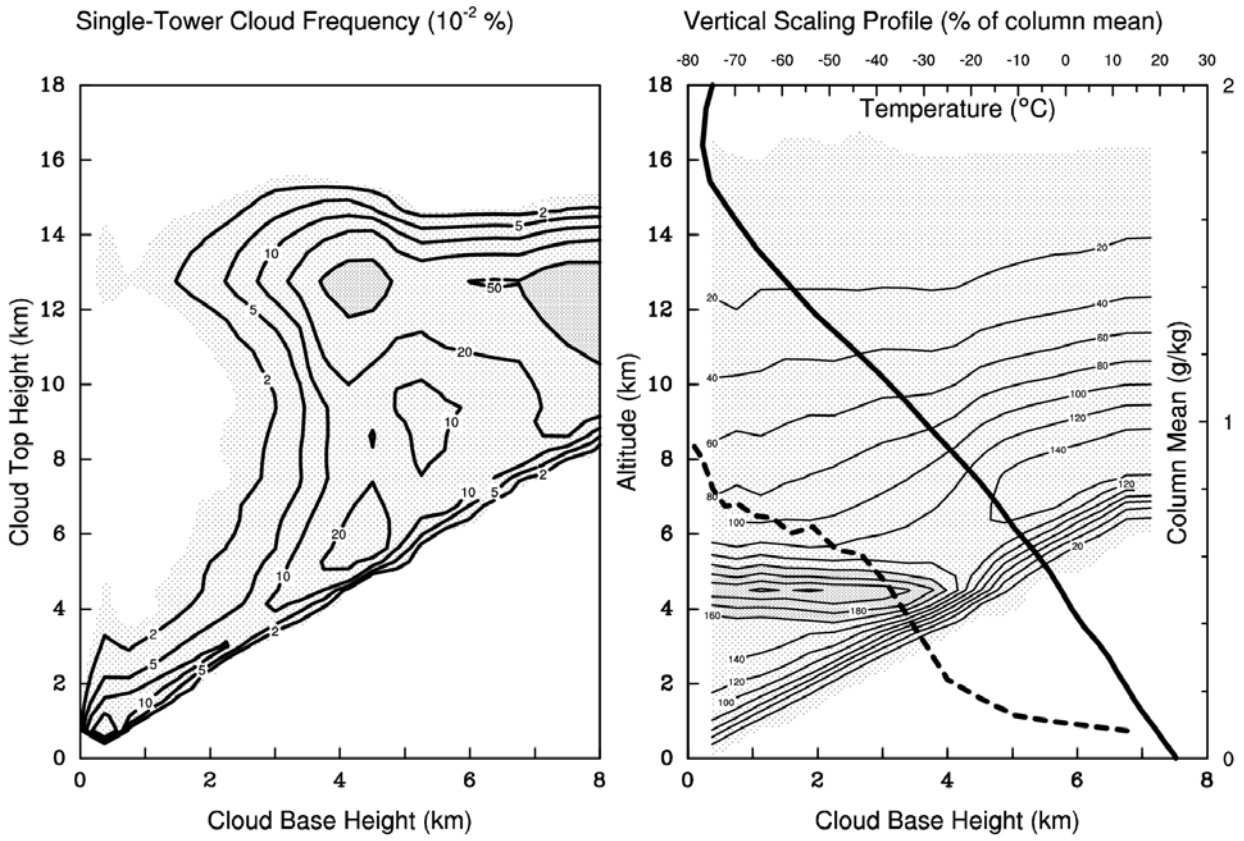

Figure 3. Statistics of a single-tower cloud simulated by the CRM over the TOGA-COARE region during December 5, 1992 - January 3, 1993. Left panel: The cloud frequency (in 10^{-4} unit) as a function of cloud base and top heights with contours at 2, 5, 10, 20, 50, and 100 units. Right panel: The cloud liquid/ice water vertical scaling profile (contours at 20 units) is defined as percentages of the column mean values (dashed line; using the lower and right scales); the domain mean temperature profile (thick solid, using the top and left scales is also shown.

characteristics in the cloud radiative forcing. This forcing could differ substantially from that using the random overlap assumption for treating the vertical cloud distribution in the CCM3. For example, as illustrated in Figure 5, the mosaic approach generates the TOA, and inversely the surface, fluxes that fluctuate from the CCM3 results in the range of ± 30 Wm^{-2} in SW cloud radiative forcing and ± 6 Wm^{-2} in LW cloud radiative forcing. Other cases, depending on the cloud cover and optical property profiles, have larger deviations and sometimes-systematic decreases or increases.

Proposed Works

1. We will conduct the CRM simulations using the large-scale forcing from the ARM intensive operational period. The CRM integrations will be evaluated against various observations, especially the ARM measurements of clouds and radiation budgets. This will establish the credibility of the CRM integrations to study subgrid cloud-radiation interactions.

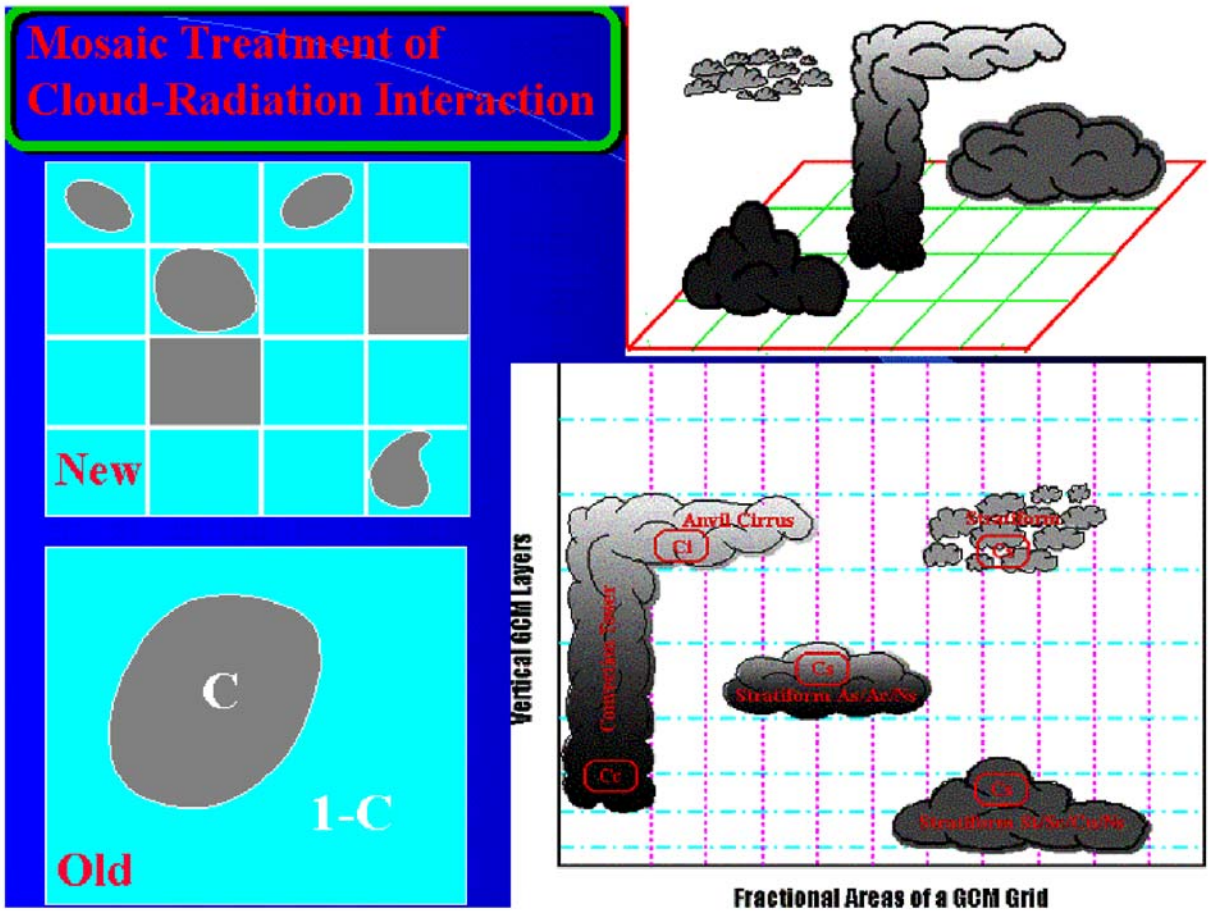

Figure 4. The schematic diagram of the mosaic subcell cloud distribution. Vertical lines divide a GCM grid into N subcell columns and horizontal lines separate model layers.

2. We will derive cloud statistics using the CRM integrations to characterize cloud geometric association (e.g., vertical overlapping) and optical property inhomogeneity (e.g., cloud liquid and ice distributions). These statistics will be in the form of probability distribution functions (PDFs) that are used by a mosaic treatment to incorporate subgrid cloud-radiation interactions.

3. We will implement the mosaic treatment with the CRM-based PDFs into the NCAR CAM and conduct the Atmospheric Model Intercomparison Project (AMIP) II integrations to quantify the climate impacts that result from subgrid cloud-radiation interactions.

Acknowledgments

This research was supported by the Biological and Environmental Research Program, U.S. Department of Energy, Grant No. DE-FG03-02ER63354. This work is part of the NCAR Clouds in Climate Program.

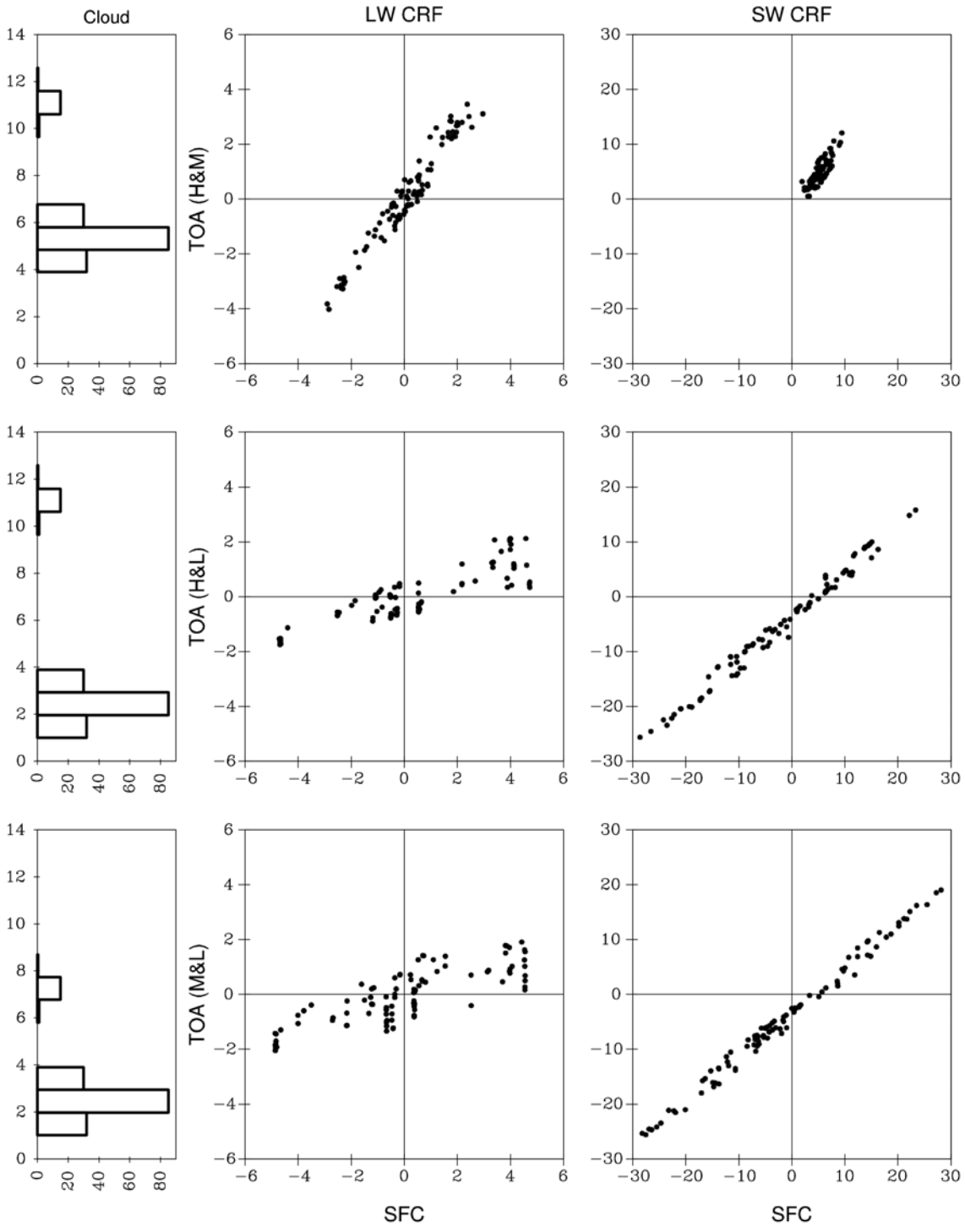

Figure 5. The stochastic cloud-radiative effects associated with the mosaic approach. The LW and SW cloud-radiative forcing (CRF; Wm^{-2}) at the TOA and on the surface (SFC) are the differences between the mosaic approach and the CCM3 random overlap scheme for the specified vertical cloud distribution (left panel). Each dot represents one of 100 mosaic calculations using a standard mid-latitude summer model atmosphere.

Corresponding Author

Dr. Xiaoqing Wu, xiaoqing@ucar.edu, (303) 497-8198

References

Ackerman, T. P., W. E. Clements, F. J. Barnes, and D. S. Renné, 1999: Tropical Western Pacific cloud and radiation testbed: Science, siting, and implementation strategies. ARM-99-004, the U.S. Department of Energy, p. 71.

Del Genio, A. D., M.-S. Yao, W. Kovari, and K. K.-W. Lo, 1996: A prognostic cloud water parameterization for global climate models. *J. Climate*, **9**, 270-304.

Dudek, M. P., S.-Z. Liang, and W.-C. Wang, 1996: A regional climate model study of the scale-dependence of cloud-radiation interactions. *J. Climate*, **9**, 1221-1234.

Fowler, L. D., and D. A. Randall, 1996: Liquid and ice cloud microphysics in the CSU general circulation model, II: Impact on cloudiness, the Earth's radiation budget, and the general circulation of the atmosphere. *J. Climate*, **9**, 530-560.

Liang, X.-Z., and W.-C. Wang, 1997: Cloud overlap effects on general circulation model climate simulations. *J. Geophys. Res.*, **102**, 11,039-11,047.

Mace, G. G., T. P. Ackerman, P. Minnis, and D. F. Young, 1998: Cirrus layer microphysical properties derived from surface-based millimeter radar and infrared interferometer data. *J. Geophys. Res.*, **103**, 23,207-23,216.

Tian, L., and J. A. Curry, 1989: Cloud overlap statistics. *J. Geophys. Res.*, **94**, 9925-9935.

Wu, S., W. W. Grabowski, and M. W. Moncrieff, 1998: Long-term behavior of cloud systems in TOGA COARE and their interactions with radiative and surface processes. Part I: Two-dimensional Modeling Study. *J. Atmos. Sci.*, **55**, 2693-2714.

Wu, X., W. D. Hall, W. W. Grabowski, M. W. Moncrieff, W. D. Collins, and J. T. Kiehl, 1999: Long-term behavior of cloud systems in TOGA COARE and their interactions with radiative and surface processes. Part II: Effects of ice microphysics on cloud-radiation interaction. *J. Atmos. Sci.*, **56**, 3177-3195.

Wu, X., and M. W. Moncrieff, 2001a: Long-term behavior of cloud systems in TOGA COARE and their interactions with radiative and surface processes. Part III: Effects on the energy budget and SST. *J. Atmos. Sci.*, **58**, 1155-1168.

Wu, X., and M. W. Moncrieff, 2001b: Sensitivity of single-column model solutions to convective parameterizations and initial conditions. *J. Climate*, **14**, 2563-2582.